Materials Research Proceedings 28 (2023) 1255-1264 https://doi.org/10.21741/9781644902479-136

Analysis of Ti-6Al-4V micro-milling resulting surface roughness for osteointegration enhancement

CAPPELLINI Cristian[1,a *], MALANDRUCCOLO Alessio[1,b], KIEM Sonja [1,c] and ABENI Andrea[2,d]

[1]University of Bergamo,Via Pasubio 7/b, 24044, Dalmine, Bergamo, Italy

[2]University of Brescia, Via Branze 38, 25123, Brescia, Italy

[a]cristian.cappellini@unibg.it, [b]alessio.malandruccolo@unibz.it, [c]sonja.kiem@natec.unibz.it, [d]andrea.abeni@unibs.it

Keywords: Ti-6Al-4V, Osseointegration, Roughness, Micro-Milling, Additive Manufacturing

Abstract. In the last period, the demand of prostheses has massively increased. To guarantee their reliability, properties of durability, biocompatibility, and osseointegration results to be mandatory. Possessing these attributes, Ti-6Al-4V alloy represents the most employed material for implants realization, and because of its microstructure, it can be manufactured by different processing methods, i.e., machining, and additive manufacturing. Considering the necessity of patient-tailored implants, and the capability of additive manufacturing to produce single batch, and complex shapes, at relatively low cost and short time, this latter represents a rewarding process. Compared to biocompatibility, that is mainly function of material chemistry, durability and osteointegration concern mostly surface roughness that affects cells growth at bone-prosthesis interface. After additive manufacturing process and prior to be inserted in the human body, a prosthetic implant is finished by machining operations, hence, the attainment of an appropriate resulting surface roughness is crucial for obtaining a successful implant. Thus, roughness forecasting capability, as a function of the employed finishing process, permits its optimization, avoiding expensive scraps. For this reason, this paper deals with the development of predictive models of surface roughness when micro-milling Ti-6Al-4V alloy specimens.

Introduction

Considering the substitution predictions of actually world-widespread prosthetic implants, such as orthopaedical and dental ones, that are estimated around 3 billion by 2030, they are requested to endure in the human body for a long period [1,2]. For guaranteeing this permanence, implants' materials must own intense resistance to corrosion in body fluids, high strength, wear and fatigue resistance, together with low density and elastic modulus [3]. Amongst metallic biocompatible materials answering to these requirements, Ti-6Al-4V titanium alloy is the most employed for bone and dental replacements [4]. This is related to its characteristics of bio-inertness [5], passivation by titanium dioxide (TiO2) layer formation [6], for avoiding inflammatory reactions, appropriate weight distribution in the human body by high strength-weight ratio [7], paramagnetism, limited stress yielding phenomena [3], osseointegration enhancement due to cementless joints creation [7], and high fatigue strength, mandatory in the normal body-cyclic load conditions [3]. Ti-6Al-4V microstructure is characterized by the coexistence of α-phase with a hexagonal close-packed (hcp) lattice and β-phase having a body-centered cubic (bcc) one, providing good ductility and making it processable by different technologies, such as forming and additive manufacturing (AM) [8]. Considering its capabilities in complex shapes realization and porosity ratios control [9], AM of titanium alloys, in particular Electron Beam Melting (EBM) methodology [10], is largely employed in biomedical field, permitting the production of optimized

and patience-tailored implants at reasonably costs [11]. AM is identified as a net-shape process, but often a milling or micro-milling operation is required for cleaning external surface defects such as lack of fusion and not-melted particles [12,13]. These processes must ensure a suitable surface roughness of the implant for facilitating osseointegration [14]. Contingently from the implant typology, roughness needs are different, and can range from values smaller than a micron up to few microns of the parameters S_a [15]. S_a parameter is usually considered instead of the R_a one since less influenced by scratches and measurement noise [16]. Beyond roughness, there are other functional parameters, such as fatigue, wear, and corrosion resistance, to be taken into account for guaranteeing implant permanence inside human body [17]. Table 1 shows these latter and their trend as a function of the implant type.

Table 1. Functional parameters qualitative values for implant permanence enhancement.

	Implant type		
Parameters	Dental implants	Bone plates and screws	Ball joints
Surface roughness	↑	↔	↓
Mechanical and fatigue resistance	↓	↔	↑
Wear resistance	↓	↑	↑
Pitting corrosion resistance	↑	↓	↓
Fretting resistance	↓	↔	↑
Crevice corrosion resistance	↓	↑	↓
Table legend: ↑ = high values; ↔ = medium values; ↓ = low values			

Pondering all these aspects, the analysis of micro-milling resulting surface roughness is essential to evaluate the capability of this process for promoting osteointegration. This study analyses the achievable roughness in micro-milling of Ti-6Al-4V EBM AM-ed specimens, with different cutting parameters. An Analysis of Variance (ANOVA) of S_a experimental results individuated the most affecting parameters, and mathematical models for S_a calculation were derived. Once validated by further micro-milling tests, these latter can be employed as predictive tools for S_a estimation starting from a set of known process parameters, or to optimize them as a function of the desired S_a values.

Materials and Methods

The analyzed results were attained form an experimental campaign of micro-milling of differently manufactured Ti-6Al-4V specimens. Two groups of cubic samples with a dimension of 10x10x10 mm^3 were processed: the first one extracted from 20 mm diameter bars resulting from rolling process, and the second one produced by EBM process, named As-received and EBM respectively. EBM specimens were fabricated with an EBM SYSTEM MODEL A2 machine (ARCAM, Designvägen 2 SE-435 33 Mölnlycke Sweden) in vacuum conditions, from ARCAM Ti-6Al-4V powders. Chemical composition, density, and particle size of these latter are reported in Table 2, where the particle size has been assessed as a function of its distribution for different percentiles (d10, d50, and d90), as indicated by ASTM B214-16 standard. Printing parameters were beam power 1250 W with a focus of 80 µm, printing speed 4530 mm/s, hatch spacing 100 µm, slice thickness 50 µm, and alternating the deposition angle amongst layers 90°. After their realization, the specimens were sonically cleaned in an acetone-isopropanol solution [18].

Cutting operations were performed on a five axis Nano Precision Machining Center KERN Pyramid Nano (Kern Micro Technik, Olympiastr. 2, D-82418 Murnau-Westried Germany) having a Heidenhain iTCN 530 numeric control. Each specimen was previously roughed by face milling it with a three flutes flat bottom mill (nominal diameter of 3 mm) at a depth of cut of 100 µm, a

cutting speed of 100 m/min, and a feed of 7.5 µm/tooth/rev for reaching a planar surface. Then, micro-milling of micro-channels along the whole length in the central part of the samples, by a two-flutes micro-mill, RIME HM79/05, was accomplished. The tool had a diameter of 0.5 mm, an edge radius of 5 µm, a helix angle of 30°, and the material was tungsten carbide (WC) coated with titanium aluminum nitride (TiAlN).

Table 2. Dimensional and chemical properties of Ti-6Al-4V powders.

Percentile of particle size distribution[1]	Particle size [µm]
d10	50
d50	68
d90	98
Powder apparent density [g/cm³]	2.57
Chemical composition [%wt]	
Al	6.42
V	3.88
O	0.13
Fe	0.18
Ti	Balance
[1] ASTM B214-16 Standard Test Method for Sieve Analysis of Metal Powders	

Micro-channels were realized maintaining a constant axial depth of cut a_p equal to 0.03 mm and changing cutting speed V_C and feed f_Z in a range of 30-50 m/min and 2-4 µm/tooth/rev respectively, following the central composite design (CCD) experimental plan [19], with an α value of 2 (Fig. 1). The CCD central point with $V_C = 40$ m/min and $f_Z = 3.0$ µm/tooth/rev was repeated three times for statistical reliability purposes [20]. The 11 tests shown in Fig. 1 were performed for both the As-received and EBM specimens, giving a total number of 22 experiments.

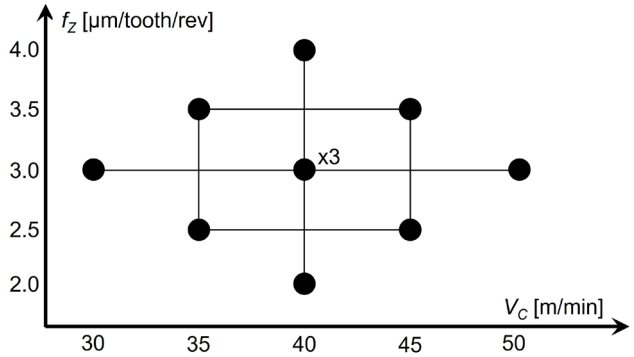

Fig. 1. The employed CCD experimental plan.

A new tool was utilized for each micro-machined channel for avoiding undesired effects of the surface roughness related to tool wear occurrence.

Surface roughness parameters S_a were measured exploiting an optical microscope, namely Mitaka PF60 (Mitaka Kohki.Co.,Ltd., Japan). Consistent with ISO 25178 standard for three-dimensional parametric definition of surface texture, irregularities' heights S_a can be evaluated by Eq. 1:

$$S_a = \frac{1}{LB}\int_0^L \int_0^B |\eta(x,y)|\, dx\, dy \quad (1)$$

where $\eta(x,y)$ is the surface irregularities deviation from base plane, L is the length and B the width of the explored section. In this work, this latter was positioned at the center of the micro-channel with $L = 0.245$ mm and $B = 2.3$ mm, with a magnification of 400x. Fig. 2 shows a S_a measurement example, while Table 3 the acquired S_a results.

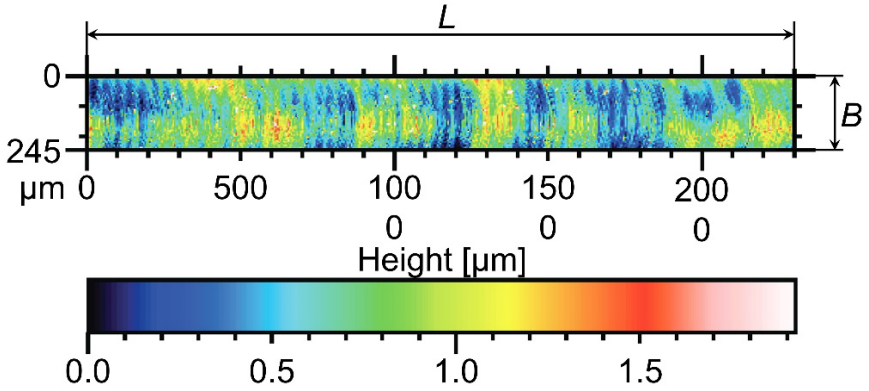

Fig. 2. Example of the acquired S_a measurement (V_C = 40 m/min, f_Z = 30 μm/tooth/rev).

Table 3. Summary of the S_a experimental values for all the tests.

V_C [m/min]	f_Z [μm/tooth/rev]	As-received S_a [μm]	EBM S_a [μm]
40	4.0	0.36	0.27
45	3.5	0.27	0.20
35	3.5	0.29	0.24
50	3.0	0.27	0.25
40	3.0	0.37	0.26
40	3.0	0.34	0.34
40	3.0	0.35	0.29
30	3.0	0.44	0.25
45	2.5	0.37	0.25
35	2.5	0.32	0.29
40	2.0	0.39	0.23

Results and Discussion

With the intent of evaluating which are the process parameters most influencing S_a, and how it is affected by their variation, an ANOVA of the whole set of experimental values, for both As-received and EBM, was performed. The ANOVA results and the related developed regression models' consistency is directly associated to data normality [21]. Therefore, for checking the normal distribution of S_a data, their probability plots were determined. These are reported in Fig. 3, where the central line denotes the cumulative probability, while the upper and lower curves delimit the 95 % confidence interval (CI) boundaries. For verifying the normality assumption, the analyzed data must remain within the CI curves and close to the probability line. Fig. 3a and 3b, representing the probability plots of As-received and EBM S_a values respectively, underline the data normality.

Analysis of As-received S_a.

Table 4 reports ANOVA results for As-received S_a values. Source column indicates the examined process parameters, where it can be observed that their single effects, interactions, and squared contributions were considered. The other columns represent the number of degrees of

freedom (DoF), the adjusted sum of squares (Adj. SS), the adjusted mean of squares (Adj. MS), the F-value, and the p-value of each source. The ANOVA individuated that the S_a value related to the parameter combination V_C = 35 m/min and f_Z = 3.5 µm/tooth/rev had a high standardized residual, indicating it as an outlier. As described in [20], the presence of outliers can be related to several factors, such as the measurer's experience, or the randomization and sequence of the measurements. Anyway, if the value of standardized residual is greater than 4 times the standard deviation, the outlier can be removed without compromising the ANOVA reliability [20]. Since the standardized residual of the outlier had a value of 2.12, 40 times the standard deviation, it was removed in the Response Surface Methodology (RSM) regression analysis.

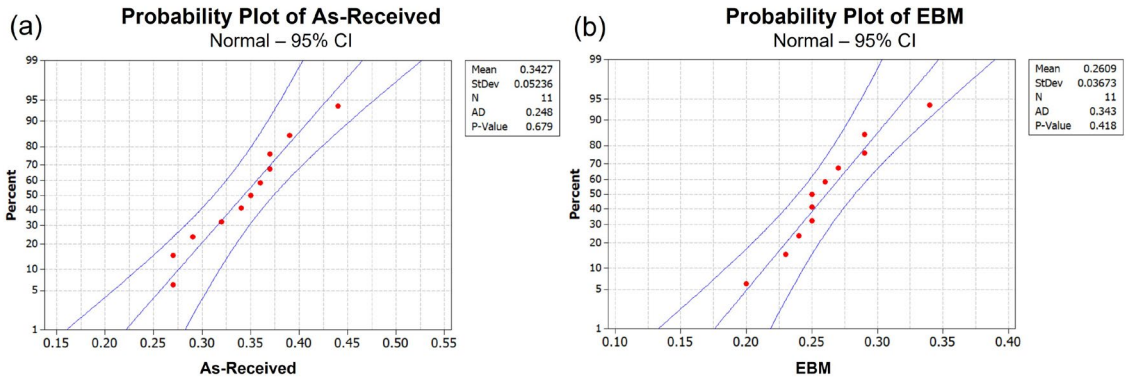

Fig. 3. Probability plots of S_a for (a) As-received, and (b) EBM specimens.

Table 4. ANOVA results for As-received S_a values.

Source	DoF	Adj SS	Adj MS	F-Value	p-Value
f_Z	1	0.000057	0.000057	0.16	0.712
V_C	1	0.015858	0.015858	43.93	0.003
$f_Z \times f_Z$	1	0.000600	0.000600	1.66	0.267
$V_C \times V_C$	1	0.000006	0.000006	0.02	0.900
$f_Z \times V_C$	1	0.008901	0.008901	24.66	0.008
Error	5	0.001444	0.000361		
Total	10	0.024360			

The assessment of the source parameter significant influence on response (S_a) is indicated by the p-value. In the common practice, in fact, if p-value is lower than the significance level, the null hypothesis H0, stating that there is no source-response relation, is rejected. Significance level is directly correlated to CI, thus, considering a CI of 95 % for the present analysis, its value is equal to 1 – 95 % = 0.05. Therefore, when p-value is lower than 0.05 the alternative hypothesis H1 is accepted, concluding that there is a statistically significant source-response relationship [21].

Table 4 results indicate that the variations of V_C and its interaction with f_Z have significant effects on S_a for the As-received material. This outcome is confirmed by the main effects plots of Fig. 4a as well, where an increase of V_C improves the surface quality, reducing the S_a value. A similar trend is also detected when considering the f_Z variation (Fig. 4b), even if a significant influence is not revealed. The surface and contour plots of Fig. 5a and 5b evidently depict the V_C - f_Z interaction effect, while report, once again, that how f_Z affects S_a is not clear. At high values of V_C, in fact, an increase of f_Z lead to a S_a reduction, but at low V_C values, S_a behavior is the opposite. Due to this, further investigations to clarify the f_Z impact are needed.

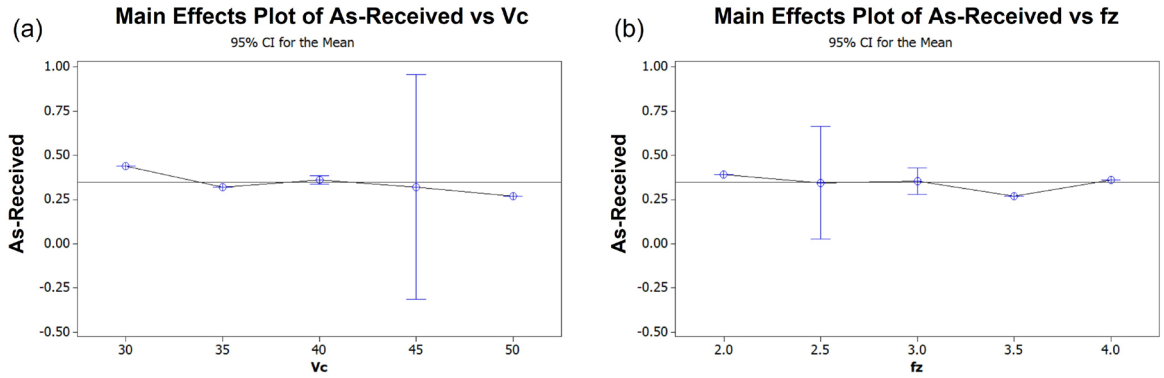

Fig. 4. Main effects plots for As-received S_a.

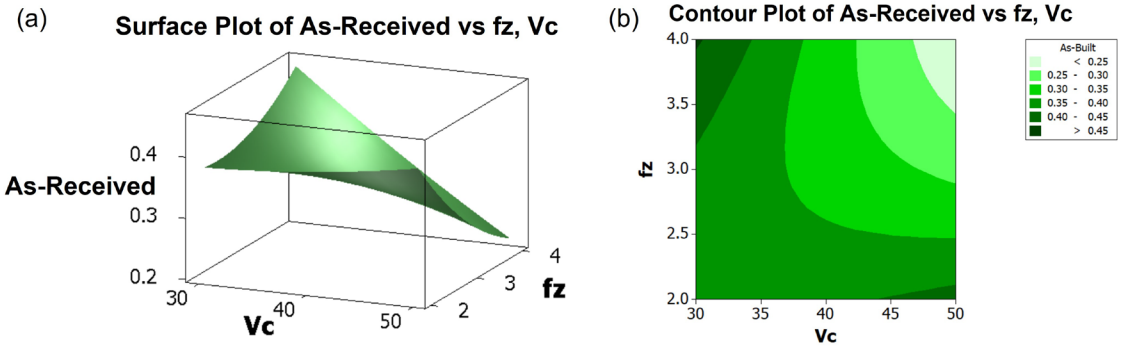

Fig. 5. Surface (a) and contour (b) plots for As-received S_a.

Analysis of EBM S_a.

The ANOVA results of S_a data for EBM micro-milled specimens are reported in Table 5.

Table 5. ANOVA results for EBM S_a values.

Source	DoF	Adj SS	Adj MS	F-Value	p-Value
f_Z	1	0.001408	0.001408	3.05	0.141
V_C	1	0.005208	0.005208	11.29	0.020
$f_Z \times f_Z$	1	0.000647	0.000647	1.40	0.290
$V_C \times V_C$	1	0.000056	0.000056	0.12	0.741
$f_Z \times V_C$	1	0.000225	0.000225	0.49	0.516
Error	5	0.6598	0.13196		
Total	10	12.7408			

Table 5 highlights that only V_C significantly influences S_a. In particular, when augmenting V_C the surface roughness decreases, and this comportment is represented by the negative slope of the related main effects plot in Fig. 6a. Feed shows an analogous behavior (Fig. 6b), but, as in the case of As-received specimens, a statistical significance of it on S_a is not detectable by ANOVA, therefore its final contribution requires to be further explored. Surface and contour plots in Fig. 7 reveal the deep effect of V_C on S_a for EBM samples, pointing to the negligible influence of f_Z, mainly at the higher V_C values.

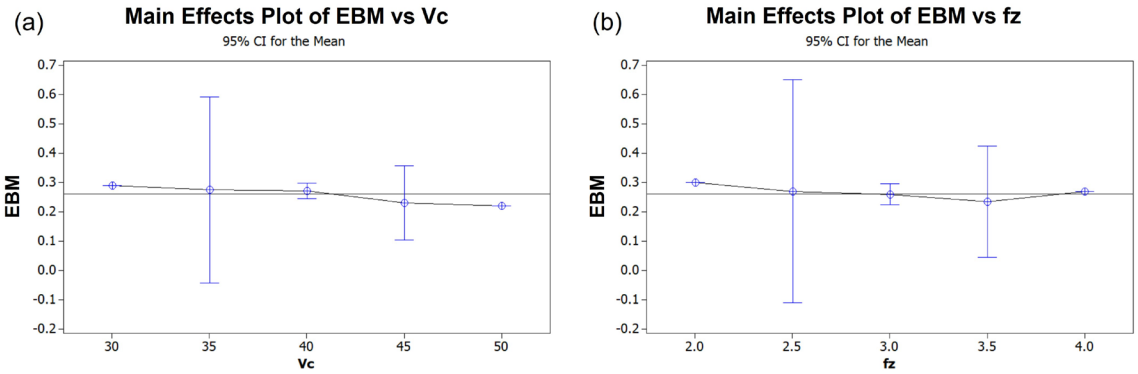

Fig. 6. Main effects plots for EBM S_a.

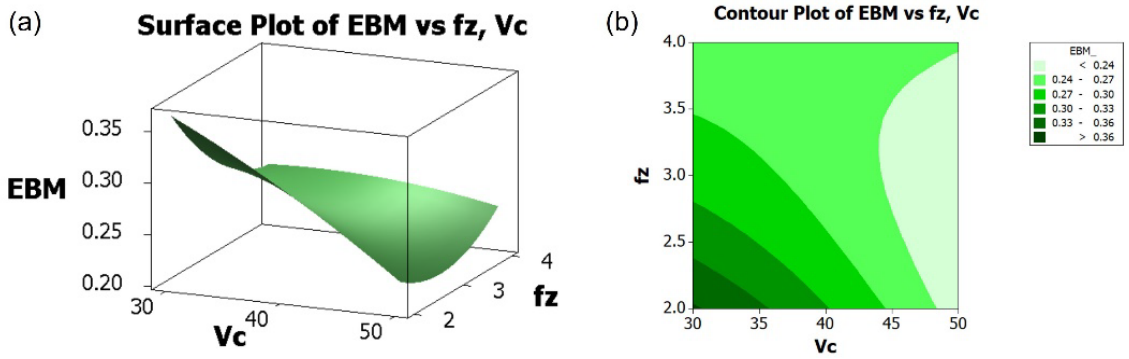

Fig. 7. Surface (a) and contour (b) plots for EBM S_a.

Response Surface Methodology (RSM) regression models.

With the aim of developing mathematical models for predicting S_a as a function of the micro-milling parameters, response surface methodology (RSM) on the whole set of S_a experimental measurements was employed. The developed regression models are reported in Eq. 2 and Eq. 3 for the calculation of As-received (S_{a_AR}) and EBM (S_{a_EBM}) resulting surface roughness respectively.

$$S_{a\_AR} = 1.9 + 0.79f_Z + 0.060V_C + 0.022f_Z^2 + 0.000023V_C^2 - 0.23f_ZV_C \quad (2)$$

$$S_{a\_EBM} = 0.23 - 0.041f_Z + 0.011V_C + 0.023f_Z^2 - 0.000068V_C^2 - 0.003f_ZV_C \quad (3)$$

The calculated S_a values for each combination of V_C and f_Z, for As-received and EBM materials, are reported in Table 6. For comparison, Table 6 shows the experimental measurements and the percentage error ($e_{\%}$) of the calculations as well.

Discussion.

ANOVA results disclose that, freely from the initial furniture status of the material, V_C heavily influences the final part surface quality. A diminution of V_C increases S_a, and this can be correlated to the vibrational effect induced by the non-homogeneous properties of the material, and to the built-up-edges (BUEs) generation at lower V_C [22]. The V_C-f_Z interaction effect can be argued considering that a f_Z increment reduces the micro-tool vibrations permitting to achieve low roughness and higher quality [23]. On the other hand, a reduction of f_Z increases the contribution of ploughing mode cutting mechanism that enlarges the surface plastic deformation lowering the paths' traces and S_a [24]. However, the analysis of further experimental tests is mandatory to clarify f_Z influence.

Table 6. Experimental and estimated S_a values comparison for As-received and EBM specimens.

V_C [m/min]	f_Z [µm/tooth/rev]	Exp S_{a_AR} [µm]	S_{a_AR} [µm]	$e_{\%\_AR}$	Exp S_{a_EBM} [µm]	S_{a_EBM} [µm]	$e_{\%\_EBM}$
40	4.0	0.36	0.369	2.4	0.27	0.258	4.3
45	3.5	0.27	0.257	4.7	0.20	0.222	11.0
35	3.5	0.29	0.452	56.0	0.24	0.278	3.1
50	3.0	0.27	0.274	1.6	0.25	0.209	5.1
40	3.0	0.37	0.351	5.2	0.26	0.257	1.2
40	3.0	0.34	0.351	3.2	0.34	0.257	7.1
40	3.0	0.35	0.351	0.3	0.29	0.257	11.4
30	3.0	0.44	0.432	1.8	0.25	0.292	0.6
45	2.5	0.37	0.378	2.1	0.25	0.259	3.5
35	2.5	0.32	0.341	6.5	0.29	0.285	1.7
40	2.0	0.39	0.378	3.2	0.23	0.302	0.7

The EBM S_a values result to be lower than the ones of As-received specimens. This is ascribable to the higher brittleness, and lower ductility, of EBM samples, related to the localized higher cooling rate of EBM process. Therefore, the superior ductility of As-received material causes an increased material adhesion on the tool cutting edge that negatively affects quality [25].

The calculation errors in Table 6 stand below the 11 %, the only exception is related to a $e_{\%}$ of 56 % related to the detected outlier, for which the significance of the value must not be taken into consideration. Overall, the low error values achieved highlight the applicability of the proposed models. Further tests need to be performed to finally validate Eq. 2 and 3 and permitting to exploit a reliable tool to forecast the attainable S_a once V_C and f_Z have been selected, or to optimize the cutting parameters as a function of the desired S_a. It should be noted that the assessment of S_a for promoting osseointegration concerns surface chemistry and morphology as well, giving the necessity of a deeper analysis to establish optimal conditions [26]. Additionally, different S_a requirements are crucial for different biomedical applications [27]. As an example, the outcomes of the accomplished micro-milling tests do not warrant to achieve the optimal combination of material, production process, and cutting parameters for a S_a value suitable for dental applications ($S_a \approx 1.5$ µm). Therefore, additional investigations should be made for analyzing the possibility of micro-machining processes employment in the dental field. Anyway, the achieved S_a values are applicable for prosthetic implants and culture cell grows.

Summary

This paper presents the study of micro-milling cutting parameters effects on the resulting surface roughness S_a as a function of different states of furniture of the material, with the aim of promoting osseointegration of prosthetic implants made of Ti-6Al-4V biocompatible alloy. The ANOVA of the data, obtained by means of an extensive experimental campaign, allowed to identify the most affecting cutting parameters, revealing V_C as the most significant. The application of RSM on data lead to the development of regression models capable to estimate S_a with good approximation, underlining their potential to predict and optimize roughness. A general increase of S_a has been observed when both V_C and f_Z decrease, even if, other tests should be performed to clarify f_Z contribution. The optimum roughness value establishment remains, in fact, a difficult task, being it not merely manufacturing process dependent, but implant application, material chemistry, mechanical and corrosion resistance related as well (Fig. 8). Consequently, ulterior studies and in vitro osseointegration tests are needed to identify the optimal topography combining all requirements.

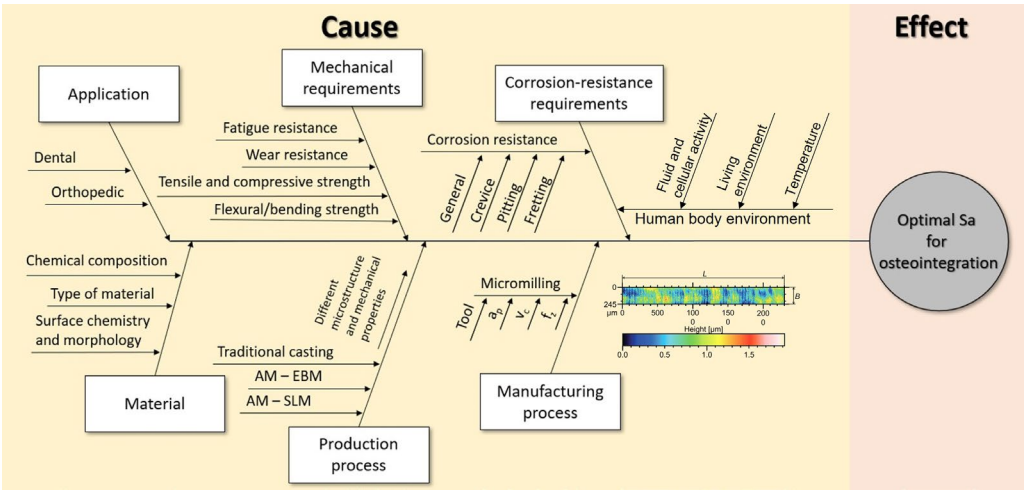

Fig. 8. Summary of influencing parameters on optimal S_a for osseointegration.

References

[1] Y.L. Hao, S.J. Li, R. Yang, Biomedical titanium alloys and their additive manufacturing, Rare Met. 36 (2016) 661-671. http://doi.org/10.1007%2Fs12598-016-0793-5

[2] M. Sarraf, G.E. Rezvani, S. Alipour, S. Ramakrishna, N.L. Sukiman, A state of the art review of the fabrication and characteristics of titanium and its alloys for biomedical applications, Biodes. Manuf. 5 (2022) 371–395. https://doi.org/10.1007/s42242-021-00170-3

[3] R.B. Heimann, Biomaterials – characteristics, history, applications, in: R.B. Heimann (Eds.), Materials for Medical Applications, Walter de Gruyter, Berlin/Boston, 2020, pp. 1-74.

[4] S.A. Aghili, K. Hassani, M. Nikkhoo, A finite element study of fatigue load effects on total hip joint prosthesis, Comput. Methods Biomech. Biomed. Eng. 24 (2021) 1545-1551. https://doi.org/10.1080/10255842.2021.1900133

[5] G.S. Kaliaraj, T. Siva, A. Ramadoss, Surface functionalized bioceramics coated on metallic implants for biomedical and anticorrosion performance-a review, J. Mater. Chem. B 9 (2021) 9433-9460. https://doi.org/10.1039/D1TB01301G

[6] P. Pedeferri, Corrosion in the human body, in: L. Lazzari, M.P. Pedeferri (Eds.), Corrosion Science and Engineering, Springer Cham, Switzerland, 2018, pp. 575-587.

[7] J.W. Nicholson, A.J. Connor, Biological interactions with materials, in: J.W. Nicholson (Eds.), The Chemistry of Medical and Dental Materials, RSC, 2020, pp. 186-226.

[8] S. Gialanella, A. Malandruccolo, Titanium and Titanium Alloys, in: Aerospace Alloys, Springer Cham, Switzerland, 2020, pp. 129-189.

[9] C. Cappellini, Y. Borgianni, L. Maccioni, C. Nezzi, The effect of process parameters on geometric deviations in 3D printing with fused deposition modelling, Int. J. Adv. Manuf. Technol. 122 (2022) 1763-1803. https://doi.org/10.1007/s00170-022-09924-4

[10] J. Tong, C.R. Bowen, J. Persson, A. Plummer, Mechanical properties of titanium-based Ti–6Al–4V alloys manufactured by powder bed additive manufacture, Mater. Sci. Technol. 33 (2017) 138-148. https://doi.org/10.1080/02670836.2016.1172787

[11] W.Y. Yeong, C.K. Chua, A quality management framework for implementing additive manufacturing of medical devices, Virtual Phys. Prototyp. 8 (2013) 193-199. https://doi.org/10.1080/17452759.2013.838053

[12] T. Özel, E. Ceretti, T. Thepsonthi, A. Attanasio, Machining Applications, in: T. Özel, P.J. Bartolo, E. Ceretti, J. De Ciurana Gay, C.A. Rodrigez, J.V. Lopes Da Silva (Eds.), Biomedical devices – Design, prototyping and manufacturing, Wiley, Hoboken, NJ, US, 2017, pp. 99-120.

[13] A. Abeni, C. Cappellini, P.S. Ginestra, A. Attanasio, Analytical modeling of micro-milling operations on biocompatible Ti6Al4V titanium alloy, Procedia CIRP 110 (2022) 8-13. https://doi.org/10.1016/j.procir.2022.06.004
[14] A. Wennerberg, T. Albrektsson, Effects of titanium surface topography on bone integration: A systematic review, Clin. Oral Implants Res. 20 (2009) 172-184. https://doi.org/10.1111/j.1600-0501.2009.01775.x
[15] T. Albrektsson, A. Wennerberg, On osseointegration in relation to implant surfaces, Clin. Implant Dent. Relat. Res. 21 (2019) 4-7. https://doi.org/10.1111/cid.12742
[16] A. Abeni, A. Metelli, C. Cappellini, A. Attanasio, Experimental optimization of process parameters in CuNi18Zn20 micromachining, Micromachines 12 (2021) 1293. https://doi.org/10.3390/mi12111293
[17] L. Lin, H. Wang, M. Ni, Y. Rui, T.Y. Cheng, C.K. Cheng, X. Pan, G. Li, C. Lin, Enhanced osteointegration of medical titanium implant with surface modifications in micro/nanoscale structures, J. Orthop. Translat. 2 (2014) 35-42. https://doi.org/10.1016/j.jot.2013.08.001
[18] P.S. Ginestra, R.M. Ferraro, K. Zohar-Haubert, A. Abeni, S. Giliani, E. Ceretti, Selective laser melting and electron beam melting of Ti6Al4V for orthopedic applications: a comparative study on the applied building direction, Materials 13 2020 5584. https://doi.org/10.3390/ma13235584
[19] Y. Men, J. Liu, W. Chen, X. Wang, L. Liu, J. Ye, P. Jia, Y. Wang, Material parameters identification of 3D printed titanium alloy prosthesis stem based on response surface method, Comput. Methods Biomech. Biomed. Eng. (2022). https://doi.org/10.1080/10255842.2022.2089023
[20] D.C. Montgomery, Design and Analysis of Experiments, 10th ed.; John Wiley & Sons, Hoboken, NJ, US, 2019.
[21] F. Concli, L. Maccioni, L. Fraccaroli, C. Cappellini, Effect of Gear Design Parameters on Stress Histories Induced by Different Tooth Bending Fatigue Tests: A Numerical-Statistical Investigation, Appl. Sci. 12 (2022) 3950. https://doi.org/10.3390/app12083950
[22] G. Kiswanto, A. Mandala, M. Azmi, T.J. Ko, The effects of cutting parameters to the surface roughness in high speed cutting of micro-milling titanium alloy Ti-6Al-4V, Key Eng. Mater. 846 (2020) 133-138. https://doi.org/10.4028/www.scientific.net/KEM.846.133
[23] A. Roushan, U. Srinivas Rao, K. Patra, P. Sahoo, Multi-Characteristics Optimization in Micro-milling of Ti6Al4V Alloy, J. Phys.: Conf. Ser. 1950 (2012) 012046. https://doi.org/10.1088/1742-6596/1950/1/012046
[24] H.K. Rafi, N.V. Karthik, H. Gong, T.L. Starr, B.E. Stucker, Microstructures and mechanical properties of Ti6Al4V parts fabricated by selective laser melting and electron beam melting, J. Mater. Eng. Perform. 22 (2013) 3872-3883. https://doi.org/10.1007/s11665-013-0658-0
[25] S.P.L. Kumar, D. Avinash, Experimental biocompatibility investigations of Ti–6Al–7Nb alloy in micromilling operation in terms of corrosion behavior and surface characteristics study, J. Braz. Soc. Mech. Sci. Eng. 41 (2019) 364. https://doi.org/10.1080/10667857.2021.1903671
[26] A. Kemény, I. Hajdu, D. Károly, D. Pammer, Osseointegration specified grit blasting parameters, Mater. Today: Proc. 5 (2018) 26622-26627.
[27] R. Krishna Alla, K. Ginjupalli, N. Upadhya, M. Shammas, R.R. Krishna, R. Sekhar, Surface roughness of implants: A review, Trends Biomater. Artif. Organs 25 (2011) 112-118.